Assessing ReFRESCO Compressible Single Phase Flow Solver Numerical Robustness

João Muralha*, Luís Eça*, and Christiaan Klaij†
*IST Técnico Lisboa, Lisbon/Portugal, †MARIN Maritime Research Institute Netherlands, Wageningen/The Netherlands
joao.muralha@tecnico.ulisboa.pt

1 Introduction

For must numerical simulations done in naval and offshore applications considering the fluids to be incompressible is a valid and reasonable approximation. Specific phenomena like slamming, sloshing and cavitation may require fluid compressibility to be taken into consideration. The goal of the present development of ReFRESCO is to modify the current flow solver to accurately solve compressible two-phase flows.

The first stage of this development was the introduction of a pressure-based single-phase flow solver. Before continuing ReFRESCO development, it is necessary to check the numerical convergence properties, i.e., the robustness (iterative errors) and order of grid convergence (discretization errors) of the solver. For this purpose, two test cases were used: the two dimensional zero pressure gradient turbulent flat plate and the two dimensional flow over a bump. These test cases were selected from NASA Langley Research Center Turbulence Modeling Resource webpage (Rumsey, 2009).

In the present work, the results, of ReFRESCO single-phase compressible flow solver are also compared to the results from CFL3D and FUN3D, which are available at Rumsey (2009).

2 ReFRESCO Flow Solver

ReFRESCO (`www.refresco.org`) is a CFD code aimed for maritime applications. The equations are discretised using a finite volume approach with cell-centered collocated variables. A face based implementation permits the use of grids with arbitrary cells geometries, as well as the use of grids with hanging nodes. Equations are linearised using Picard's method.

The flow solver used in the present work is a pressure based solver of the compressible Navier-Stokes equations. Mass conservation is ensured by means of a pressure-correction equation based on the SIMPLE algorithm. The pressure-velocity-density used in the derivation of the pressure correction equation is described in Ferziger and Perić (2001) and Muralha et al. (2018). The compressible Navier-Stokes equations require a relation between temperature, density and pressure, that in the present solver is given by the perfect gas equation of state.

2.1 Turbulence modelling in compressible flows

In compressible turbulent flows, density and temperature fluctuations must be taken into account. If the Reynolds average are applied to compressible flows the complexity of the closure approximations would increase in comparison to incompressible flows, for example, a triple correlation involving density and velocities fluctuations appears. The time-averaged equations can be simplified by applying a density-weighted averaging procedure, known as Favre averaging (Wilcox, 1998). It is important to note that this type of averaging procedure only removes the density fluctuations from the averaged equations, i.e., it is a mathematical simplification.

The steady Favre averaged mean conservation equations are:

$$\frac{\partial}{\partial x_i}\left(\overline{\rho}\tilde{u}_i\right) = 0 \tag{1a}$$

$$\frac{\partial}{\partial x_j}\left(\overline{\rho}\tilde{u}_j\tilde{u}_i\right) = -\frac{\partial \overline{p}}{\partial x_i} + \frac{\partial}{\partial x_j}\left[\overline{\tau}_{ij} - \overline{\rho u_j'' u_i''}\right] \tag{1b}$$

$$\frac{\partial \overline{p}}{\partial t} + \frac{\partial}{\partial x_j}\left[\overline{\rho}\tilde{u}_j\left(c_p\tilde{T} + \frac{1}{2}\tilde{u}_i\tilde{u}_i\right) + \tilde{u}_j\frac{1}{2}\overline{\rho u_i'' u_i''}\right] = \frac{\partial}{\partial x_j}\left[-\overline{q_j} - c_p\overline{\rho u_j'' T''} + \overline{\tau_{ij}u_i''} - \frac{1}{2}\overline{\rho u_j'' u_i'' u_i''}\right] + \frac{\partial}{\partial x_j}\left[\tilde{u}_i\left(\overline{\tau}_{ij} - \overline{\rho u_i'' u_j''}\right)\right] \quad (1c)$$

where u_i, ρ, p, T and c_p represent the i$^{\text{th}}$ component of the velocity vector, density, pressure, temperature and specific heat at constant pressure and $\overline{\tau_{ij}}$ and q_j are given by:

$$\overline{\tau}_{ij} = \mu\left(\frac{\partial \tilde{u}_i}{\partial x_j} + \frac{\partial \tilde{u}_j}{\partial x_i}\right) - \frac{2}{3}\mu\frac{\partial \tilde{u}_k}{\partial x_k}\delta_{ij},\ \overline{q}_j = -\kappa\frac{\partial \tilde{T}}{\partial x_j}$$

with μ and κ being the dynamic viscosity, which is calculated by Sutherland's law, and thermal conductivity coefficient. The overline denotes Reynolds average and the tilde represents mass-averaged.

The Favre averaged momentum equations take the same form as the momentum Reynolds averaged equations and require the term $\tau_{ij} = -\overline{\rho u_j'' u_i''}$ to be modelled. This term is modelled using Boussinesq approximation:

$$\tau_{ij} = -\overline{\rho u_j'' u_i''} = \mu_t\left(\frac{\partial \overline{u}_i}{\partial x_j} + \frac{\partial \overline{u}_j}{\partial x_i}\right) - \frac{2}{3}\mu_t\frac{\partial \overline{u}_k}{\partial x_k}\delta_{ij} - \frac{2}{3}\overline{\rho}k\delta_{ij} \quad (2)$$

where $k = (1/2)\,\overline{u_i'' u_i''}$ is the kinetic energy of the fluctuating field and μ_t is the eddy viscosity.

In the energy equation the following terms require modelling:

$$c_p\overline{\rho u_j'' T''} \quad \overline{\tau_{ij}u_i''} \quad -\frac{1}{2}\overline{\rho u_j'' u_i'' u_i''}$$

The turbulent heat flux vector, first term starting from the left, is modelled using Reynolds analogy:

$$c_p\overline{\rho u_j'' T''} = -\frac{\mu_t c_p}{Pr_t}\frac{\partial \tilde{T}}{\partial x_j} \quad (3)$$

where Pr_t is the turbulent Prandtl number that is considered constant, 0.90 for air.

The remaining two terms, molecular diffusion and turbulent transport, are usually ignored, which is a good approximations for flows up to supersonic Mach number range.

Eddy viscosity is calculated using Spalart-Allmaras one equation turbulence model. According to Allmaras et al. (2012), the turbulence model formulation implemented in ReFRESCO is valid for both incompressible and compressible flows, so no significant changes were made.

3 Test Cases

As mentioned in Section 1, the two cases used to test the solver robustness are the steady state flow over a flat plate and over a bump. These test cases are part of NASA Langley Research Center Turbulence Modeling Resource verification case list, that provides information about each test case domain size and boundary conditions. Results for two CFD codes (CFL3D and FUN3D) in sets of geometrically similar grids, as well as the grid sets, are available. For both cases, the flow has an undisturbed Mach number (M_∞) of 0.2 and a temperature (T_∞) of 300K. The fluid is considered to be a perfect gas with specific heat ratio of 1.4 and Prandtl number equal to 0.72. The flow over the flat plate has a Reynolds number based on unit length ($L = 1$ m) equal to 5×10^6, while for the flow over the bump the Reynolds number is 3×10^6.

Figure 1 illustrates the domain of both test cases and indicates the boundary conditions used at each boundary. Form Fig. 1a, it is possible to see that the plate extends from $x = 0$ m to $x = 2$ m, the inlet is situated at $x = -0.3333$ m and the outlet coincides with the end of the plate. The domain used for the flow over a bump is considerably larger than for the flat plate. The inlet and outlet are located 25 meters apart from the beginning and end of the bump and the top boundary is located at $y = 5$ m, giving a domain height 100 times larger than the bump height. Although large, these type of dimensions are typical of compressible flow simulations. The bump starts at $x = 0$ m and ends at $x = 1.5$ m.

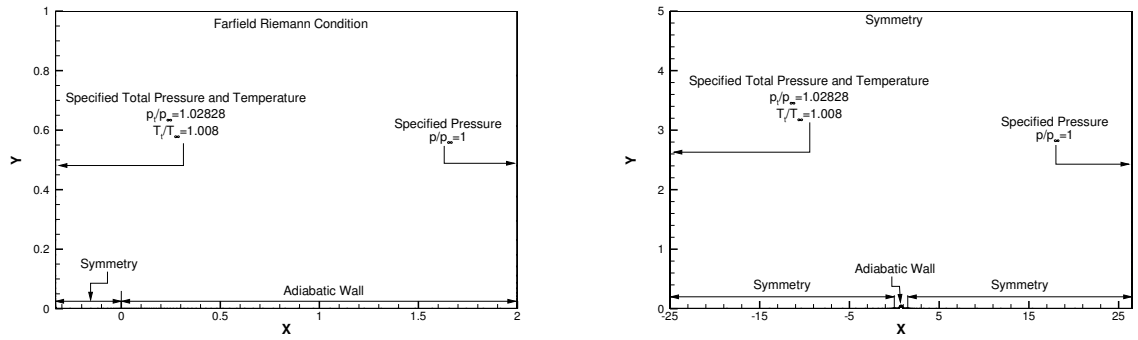

(a) Flat Plate (b) Bump

Fig. 1: Illustrations of the domain and applied boundary conditions used in the simulation of flow over a flat plate (left) and over a bump (right), as specified in the Turbulence Modeling webpage.

For both cases, the inlet flow is considered to be isentropic and total pressure, p_T, and total temperature T_T are specified, as well as the ratio between turbulent kinetic viscosity and the fluid kinetic viscosity ($\nu_{t,\infty}/\nu = 0.214038$). The implementation of the total pressure boundary condition in pressure based solvers is fully described by Ferziger and Perić (2001). At the outlet, pressure is specified and all other quantities are extrapolated from the interior cell, with exception of density. It is calculated based on the specified pressure and on the extrapolated temperature values from the equation of state (Rudy and Strikwerda, 1981). In the flat plate case a far-field Riemann boundary condition is used at the domain top. This boundary condition specifies variables according to one dimensional Riemann invariants of the Euler equations, see Hirsch (1991) for detailed explanation. For all remaining boundaries a symmetry boundary condition is applied.

4 Numerical Settings

The discretisation of the convective and diffusive terms of all transport equations was performed using second order schemes, limited QUICK for the convective term and Gauss theorem for gradient calculation. The simulations were stopped when the L_∞ norm of the normalised residuals of all solved equations were inferior to 10^{-8} for the flow over a flat plate and 10^{-7} for the flow over a bump.

The grids are illustrated in Fig. 2. The number of cells of the grids used in the flat plate case ranges from 816 to 208896, while on the bump case it ranges from 3520 to 901120. The maximum dimensionless near-wall cell size, y^+_{max}, is inferior to 1.15 in the flat plate grids and 0.75 in the bump grids.

For both test cases sets of five geometrically similar grids were used to estimate the numerical uncertainty and the order of grid convergence, p, based on the procedure introduced by Eça and Hoekstra (2014).

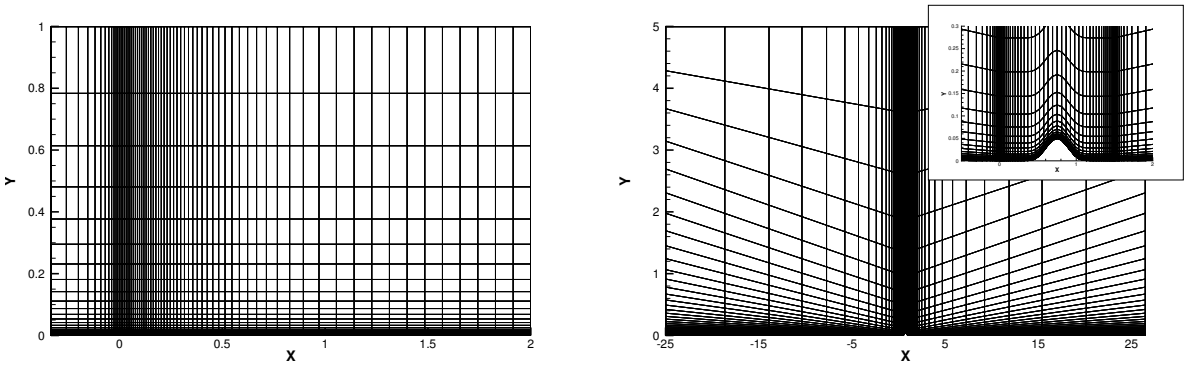

(a) Flat Plate (b) Bump

Fig. 2: Grid topology used in the simulations.

5 Iterative Convergence

Iterative convergence of the flow solver is illustrated in Fig. 3, that presents the L_∞ norm of the normalised residuals as a function of the iteration counter. The data show that the convergence of the momentum and energy equations is noisy. The origin of the noise in the convergence is the inlet boundary condition (specified total pressure and total temperature). In this type of boundary condition velocity, temperature and density are calculated at every iteration to comply with specified values of total pressure and total velocity and the perfect gas model. Figure 4 shows the iterative convergence behaviour for the simulation run using the same grid as in Fig. 3b, but with velocity, temperature and density specified at the inlet boundary. The change in inlet boundary condition will affect the obtained results, but as the domain is relatively large the change in results is small (see Section 6).

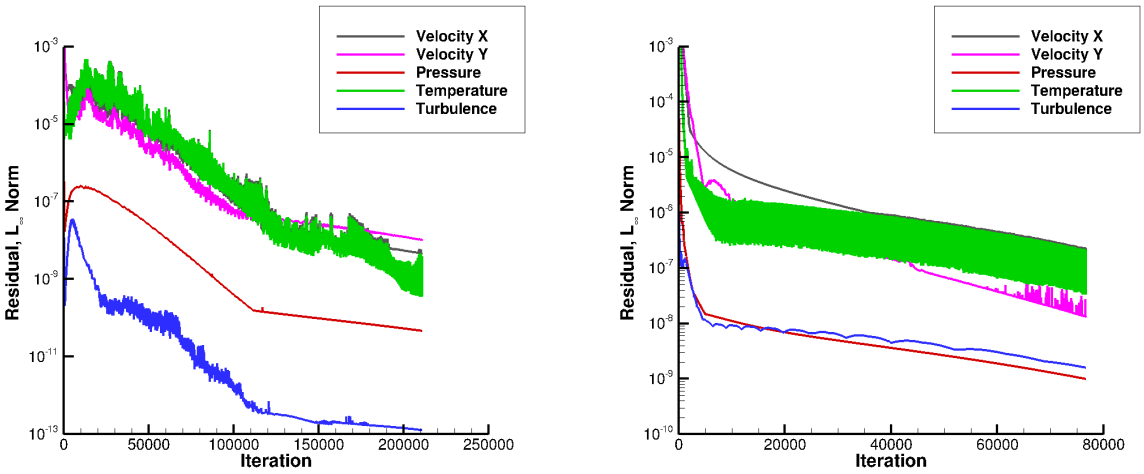

(a) Flat plate, grid with 544×384 cells.

(b) Bump, grid with 352×160 cells.

Fig. 3: Evolution of the L_∞ norm of the residuals for the simulation of flow over a flat plate and over a bump.

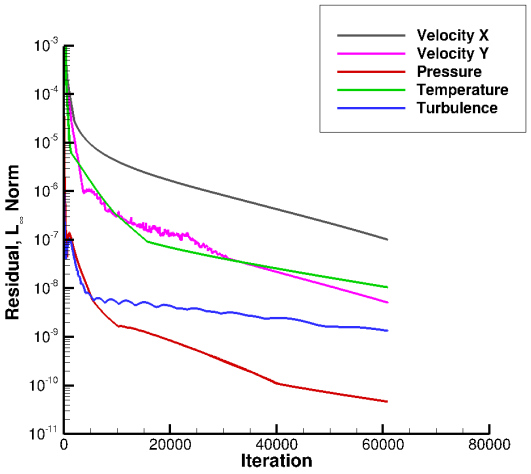

Fig. 4: L_∞ norm of the residuals for the bump case simulated in a grid with 352×160 cells and specifying velocity, temperature and density as inlet boundary conditions.

6 Grid Convergence

The select quantities of interest to determine the grid convergence properties of ReFRESCO include force coefficients (integral quantities) and skin friction coefficient (local quantities). For all the selected quantities, results obtained with CFL3D and FUN3D (density based flow solvers) in the same grids are available at Rumsey (2009). Table 1 compares the friction coefficients obtained in the ReFRESCO simulations (last line) with the results available for CFL3D and FUN3D. The friction coefficient for the

flow over a flat plate is calculated at approximately $x = 0.97$ m and the frictions coefficients for the bump case are calculated at approximately $x = 0.63$ m (upstream from bump peak, $C_{f,u}$), $x = 0.75$ m (bump peak, $C_{f,p}$) and $x = 0.87$ m (downstream from bump peak, $C_{f,d}$). The results obtained for the integral quantities are presented in Table 2. These tables show that ReFRESCO results are in good agreement with those determined by CFL3D and FUN3D.

Table 1: Results obtained using the finest grid for the local quantities of interest.

Code	Flat Plate	Bump		
	$C_{f,x} \times 10^{-3}$	$C_{f,u} \times 10^{-3}$	$C_{f,p} \times 10^{-3}$	$C_{f,d} \times 10^{-3}$
CFL3D	2.7056	5.1852	6.1494	2.6777
FUN3D	2.7054	5.1869	6.1514	2.6808
ReFRESCO (p_T and T_T)	2.7079	5.1931	6.1597	2.6870
ReFRESCO (u, T and ρ)	-	5.2126	6.1614	2.6915

Table 2: Results obtained using the finest grid for the integral quantities of interest.

Code	Flat Plate	Bump			
	$C_D \times 10^{-3}$	$C_D \times 10^{-3}$	$C_{D,v} \times 10^{-3}$	$C_{D,p} \times 10^{-4}$	$C_L \times 10^{-2}$
CFL3D	2.8599	3.5724	3.1907	3.8170	2.4900
FUN3D	2.8525	3.5611	3.1787	3.8231	2.4942
ReFRESCO (p_t and T_t)	2.8621	3.5758	3.1948	3.8102	2.4975
ReFRESCO (u_i, T and ρ)	-	3.5796	3.1992	3.9038	2.4981

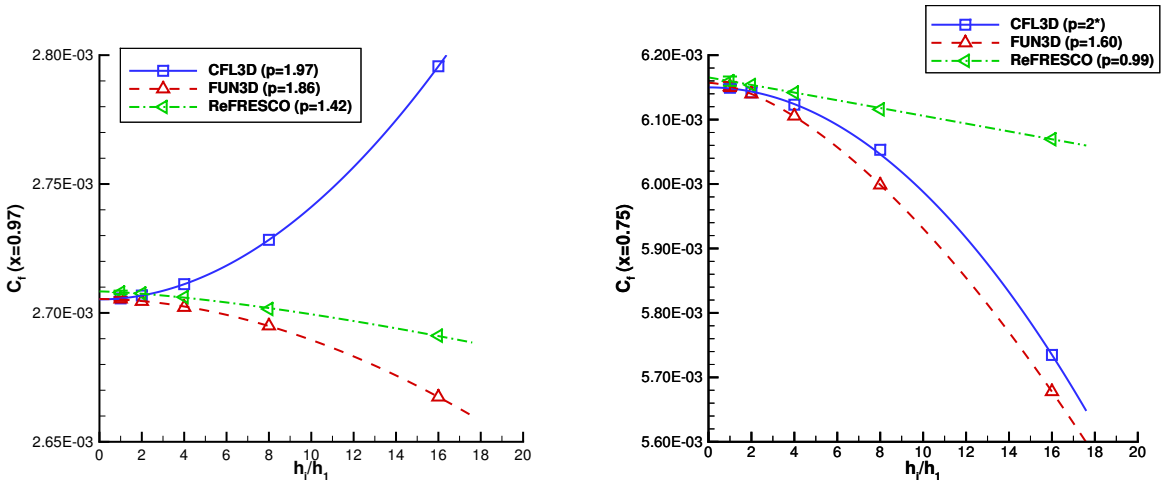

(a) Flat Plate, C_f at location x=0.97

(b) Bump, C_f at bump peak

Fig. 5: Grid convergence of the friction coefficient, C_f, and of the drag coefficient, C_D

Figure 5 illustrates the grid convergence of the friction coefficient for the flat plate (left plot) and bump (right plot) cases. Although second order convergence was achieved for manufactured solutions (laminar flow), for these test cases observed orders of grid convergence are lower than 2, with the bump test case leading to $p = 1$. The turbulence model might be responsible for the reduction of the observed order of grid convergence. As illustrated in Eça et al. (2018), the values of p obtained with the incompressible solver depend on the value of y^+. Nonetheless, the error constant obtained with ReFRESCO is smaller than those derived from the CFL3D and FUN3D data. Therefore, although observed p is larger for CFL3D and FUN3D than for ReFRESCO, the change in the solutions with grid coarsening is smaller for ReFRESCO than for the other two flow solvers.

7 Conclusions

This paper presents a study on the numerical convergence properties of ReFRESCO single phase compressible flow solver. To conduct this analysis two test cases were selected from NASA Langley Research Center Turbulence Modeling Resource webpage (Rumsey, 2009): the flow over a flat plate and over a bump. Iterative convergence properties are illustrated for the two test cases using the L_∞ norm of the normalised residuals. Observed orders of grid convergence are determined for skin friction coefficients (local flow quantities) and force coefficients (integral flow quantities). The selected quantities of interest are compared with the results of two density based solvers (CFL3D and FUN3D) available in the open literature.

Iterative convergence is significantly affected by inlet boundary conditions based on total temperature and total pressure, which originates oscillations in the convergence history and the need to use low under-relaxation parameters. Iterative convergence is improved when velocity, density and temperature are imposed at the inlet. However, such boundary condition requires a location of the inlet boundary sufficiently upstream to impose undisturbed flow conditions. Results obtained for the flow over a bump showed similar results for the two alternatives.

A good agreement between ReFRESCO, CFL3D and FUN3D solutions was obtained, but the observed order of grid convergence obtained with ReFRESCO is lower than that exhibited by the other two solvers. On the other hand, the error constant of the ReFRESCO solution less sensitive to grid coarsening.

As for the tests reported in Muralha et al. (2018) performed with manufactured solutions, the present study suggests that the choice and implementation of the boundary conditions has a decisive influence on the numerical convergence properties of the pressure based compressible flow solver.

Acknowledgements

The authors acknowledge the financial support of Fundação para a Ciência e Tecnologia throught a PhD grant attributed to the first author under the Bolsas de Doutoramento program. This research is also partly funded by the Dutch Ministry of Economic Affairs.

References

Allmaras, S. R., Johnson, F. T., and Spalart, P. R. (2012). Modifications and Clarifications for the Implementation of the Spalart-Allmaras Turbulence Model. In *Seventh International Conference on Computational Fluid Dynamics (ICCFD7)*, pages 1–11.

Eça, L. and Hoekstra, M. (2014). A procedure for the estimation of the numerical uncertainty of CFD calculations based on grid refinement studies. *Journal of Computational Physics*, 262:104–130.

Eça, L., Pereira, F. S., and Vaz, G. (2018). Viscous flow simulations at high Reynolds numbers without wall functions: Is $y^+ \simeq 1$ enough for the near-wall cells? *Computers & Fluids*, 170:157–175.

Ferziger, J. H. and Perić, M. (2001). *Computational Methods for Fluid Dynamics*. Springer-Verlag GmbH, 3rd edition.

Hirsch, C. (1991). *Numerical Computation of Internal and External Flows*, volume 2. John Wiley & Sons Ltd.

Muralha, J., Eça, L., and Klaij, C. (2018). Application of the SIMPLE Algorithm to a Manufactured Subsonic Flow. In *NuTTS*.

Rudy, D. H. and Strikwerda, J. C. (1981). Boundary Conditions for Subsonic Compressible Navier-Stokes Calculations. *Computers & Fluids*, 9(3):327–338.

Rumsey, C. (2009). Turbulence Modelling Resources.

Wilcox, D. C. (1998). *Turbulence Modeling for CFD*. DCW Industries, 2nd edition.